Supplementary material for:

Spin-orbit Coupling Induced Circular-polarization-selective Transmission in a Helical Tape Waveguide

Yahong Liu, [1, 2,*] Qinghua Guo, [2,3] Hongchao Liu,[2] Congcong Liu,[1] Kun Song,[1] Biao Yang,[2] Quanwen Hou,[1] Xiaopeng Zhao,[1] Shuang Zhang[2,] and Miguel Navarro-Cía,[2,*]

[1] Department of Applied Physics, Northwestern Polytechnical University, Xi'an, 710129, China.

[2] School of Physics and Astronomy, University of Birmingham, Birmingham, Edgbaston, B15 2TT, UK.

[3] College of Optoelectronic Engineering, Shenzhen University, Shenzhen, 518060, China.

[*]Correspondence and requests for materials should be addressed to Y. L. (email: yhliu@nwpu.edu.cn), or M. N.-C.(email: m.navarro-cia@bham.ac.uk).

I. PROPOSED HTW WITH DIFFERENT SLIT WIDTH *s*

Figures S1(a,b) are the simulated transmission and reflection coefficients for different slit widths of s = 1, 2, 3, 4, and 5 mm, respectively. Figure S1(a) shows that a very high transmission of nearly 100% can be observed at a broadband frequency range for RCP incident electromagnetic wave. When LCP wave is incident on the HTW, the transmission is 0.81, 0.61, 0.44, 0.33 and 0.21 at 9 GHz for s = 1, 2, 3, 4 and 5 mm, respectively. Hence, the transmission decreases with the increasing of the slit width s. Figure S1(b) shows that the reflection is small for both LCP and RCP incident waves irrespective of s.

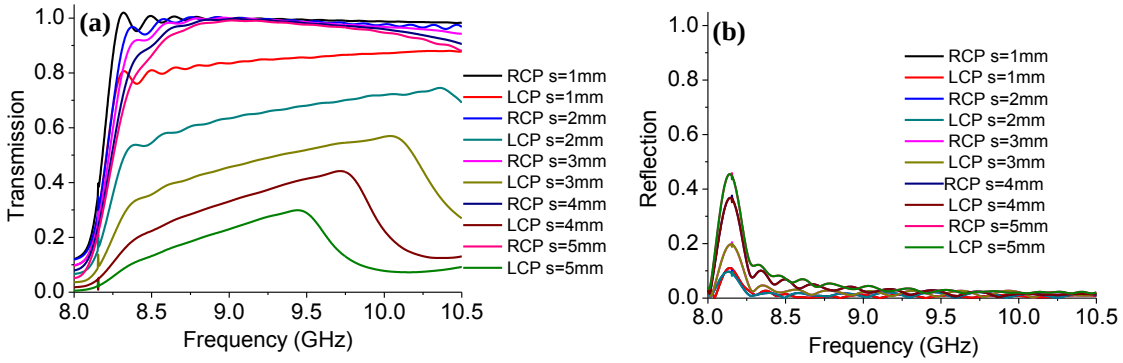

FIG. S1. Simulated (a) transmission and (b) reflection coefficients for different slit widths s = 1, 2 , 3, 4, and 5 mm. The other parameters of the HTW are: l = 290 mm, d = 21.6 mm, t = 0.5 mm, w = 15 mm, and n = 14.

Figure S2 presents the simulated electric field distributions for different slit widths at 9 GHz. It can be observed that the power is well confined in the HTW and little power leaks from the helical slits for RCP incident wave. Therefore, a very high transmission is achieved for RCP case. The results are consistent with the transmission spectra shown in Fig. S1(a). However, when LCP wave is incident on the HTW, the power leaks out through the helical slit. As expected, the leakage radiation is increased for wider slit (i.e., larger s). Therefore, the transmission decreases with the increasing of

s for LCP incident wave.

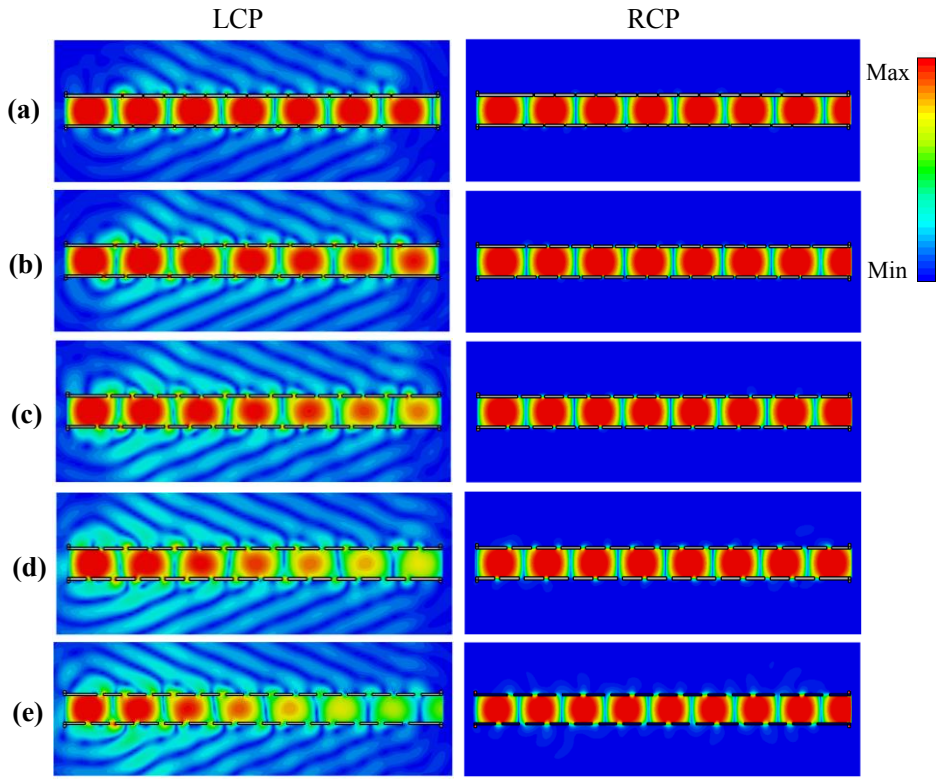

FIG. S2. Simulated electric field distributions at $x = 0$ plane for different slit widths of (a) $s = 1$ mm, (b) $s = 2$ mm, (c) $s = 3$ mm, (d) $s = 4$ mm, and (e) $s = 5$ mm at 9 GHz.

Figure S3(a) shows the far-field radiation patterns at 9 GHz for LCP wave incident into the HTW. The observed two main lobe radiation directions are centered at 66.5° and 293.5°, respectively. The main lobe magnitude increases with the increasing of *s*. The result indicates that the radiation increases with the increasing of *s* for LCP wave, which has a good agreement with the electric field distributions and transmission spectra. The far field radiation patterns for RCP incident wave as presented in Fig. S3(b) show the main lobe is centered at 0°, and the magnitudes for different slit widths are almost the same (around 6). This independence to *s* is due to the minimal leakage through the helical slit (i.e., the structure acts as a – slow-wave – transmission line).

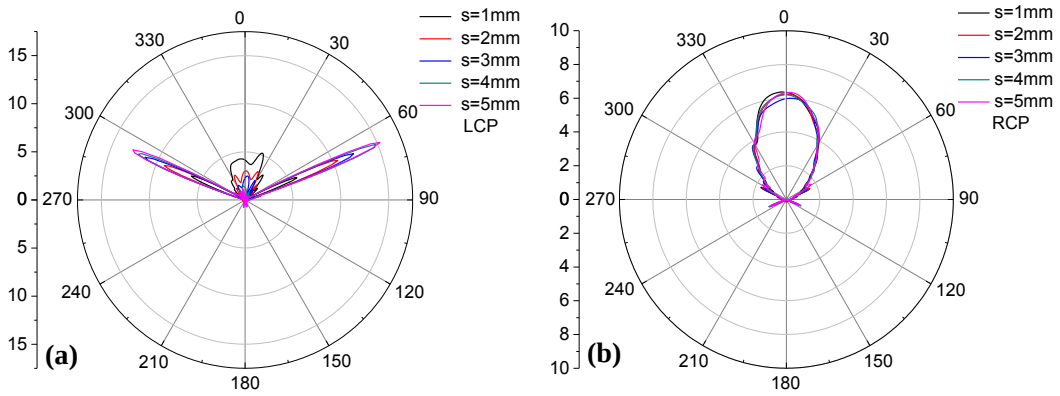

FIG. S3. Simulated far-field radiation patterns (φ = 90°, linear scale) of different slit width *s* for (a) LCP and (b) RCP waves at 9 GHz.

To clearly demonstrate the radiation origin of the HTW, Fig. S4 presents the simulated electric field vector distributions of the HTW. For LCP incident wave, Fig. S4(a) shows that the electric field at the slit oscillates along the z-direction. The proposed structure can be regarded as a phased dipole array along the *z*-direction, resulting in radiation. When RCP wave is incident on the HTW, as displayed in Fig. S4(b), the electric field of the slit is similar to that of secondary dipoles, it is a nonradiation mode. Therefore, the power is confined in the waveguide for RCP incident case.

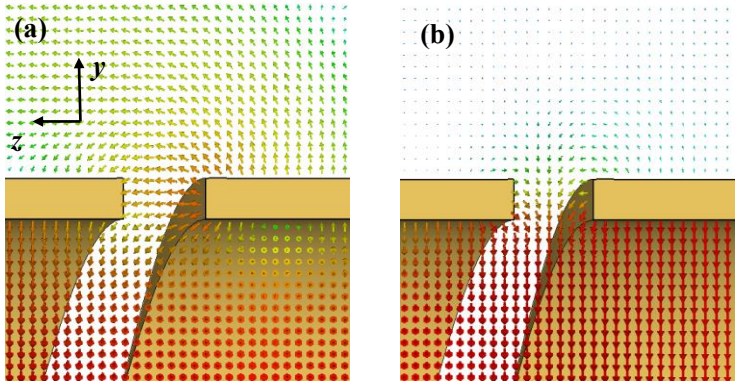

FIG. S4. (a) Partial enlarged electric field vector distributions at $x = 0$ plane for (a) LCP and (b) RCP incident waves at 9 GHz.

II. PROPOSED HTW WITH DIFFERENT TURNS *n*

We demonstrate the performances of the HTW with different *s*. Besides that, we also investigate the performances of the HTW with different turns of *n* = 14, 20, 25, and 30. Figure S5 displays the simulated transmission and reflection coefficients. It is clear that a complete transmission is observed as RCP electromagnetic wave is incident on the HTW. However, for the LCP incident wave, the transmissions are 0.33, 0.21, 0.14, and 0.097 at 9 GHz for *n* = 14, 20, 25, and 30, which indicates the transmission decreases with the increasing of *n*. Such transmission results are significant in the sense that the proposed HTW can be used to distinguish the circular handedness of incident electromagnetic wave.

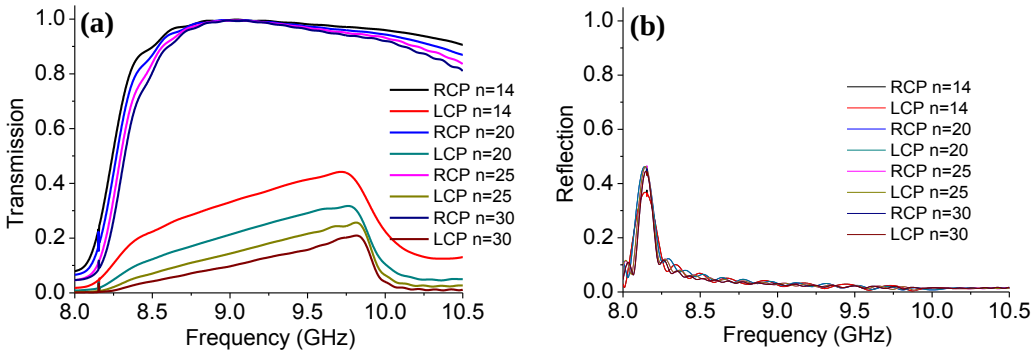

FIG. S5. Simulated (a) transmissions and (b) reflections for different turns of *n* = 14 with *l* = 290 mm, *n* = 20 with *l* = 400 mm, *n* = 25 with *l* = 500 mm, and *n* = 30 with *l* = 600 mm). The other parameters of the HTW are: *d* = 21.6 mm, *t* = 0.5 mm, *w* = 15 mm, and *s* = 4 mm.

The simulated electric field distributions for different turns *n* are shown in Fig. S6. It can be observed that the electromagnetic wave is confined completely in the helical waveguide and little electromagnetic wave is leaked from the silts for RCP wave incident on the HTW. Therefore, a very high transmission is obtained for RCP incidence wave as expected. However, electromagnetic wave

leaks from the silts and the leaky energy increases with the increasing of *n* for LCP incident wave. Therefore, the transmission becomes lower with the increasing of *n*.

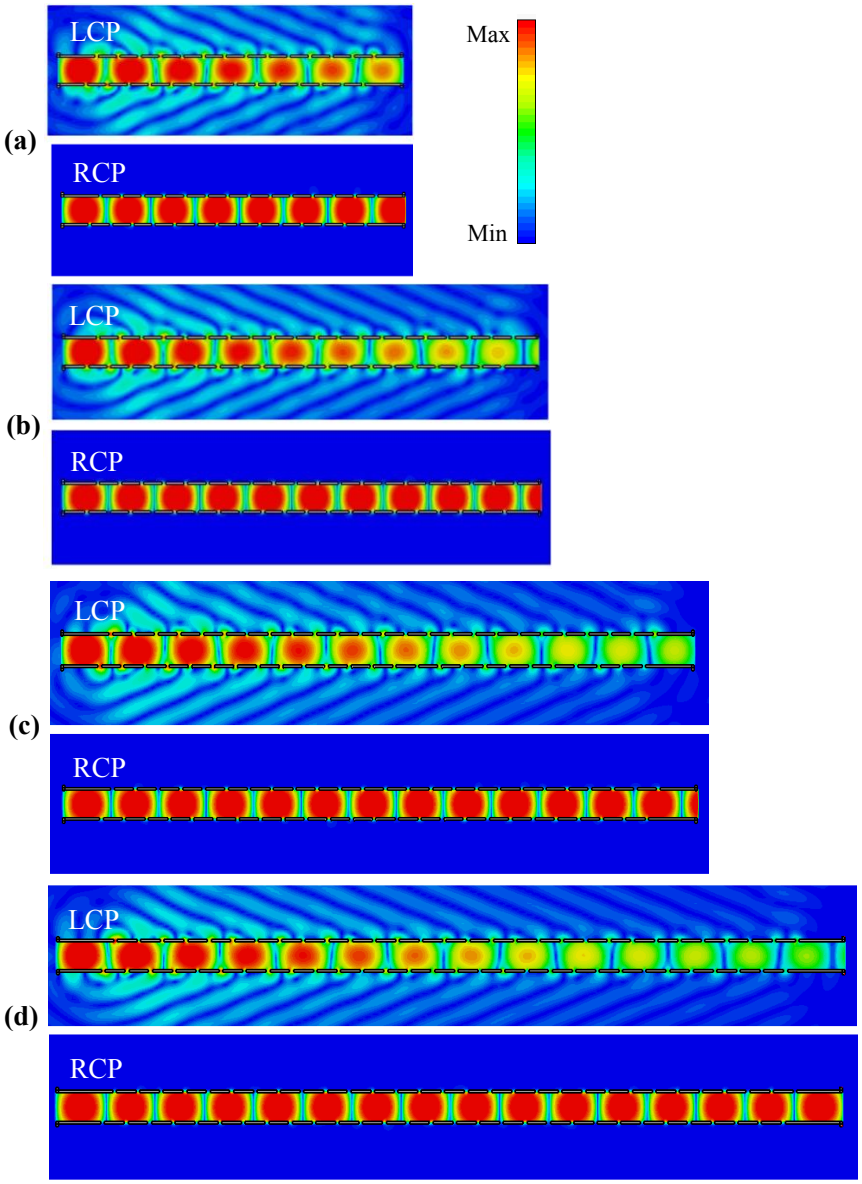

FIG. S6. Simulated electric field distributions at $x = 0$ plane for different turns *n* of (a) $n = 14$, (b) $n = 20$, (c) $n = 25$, and (d) $n = 30$ at 9 GHz.

Figure S7 presents the simulated far-field radiation patterns of the different *n* at 9 GHz. As shown in Fig. S7(a), the main lode magnitude for LCP incidence wave increases with the increase of *n*. The result reveals that the radiation increases with the increasing of *n* for LCP incident wave. In

Fig. S7(b), the far field radiation patterns for RCP incidence wave show the main lobe magnitude for different *n* is almost the same because little power is radiated through the slits. The far-field radiation results are well consistent with the electric field distributions and transmission spectra.

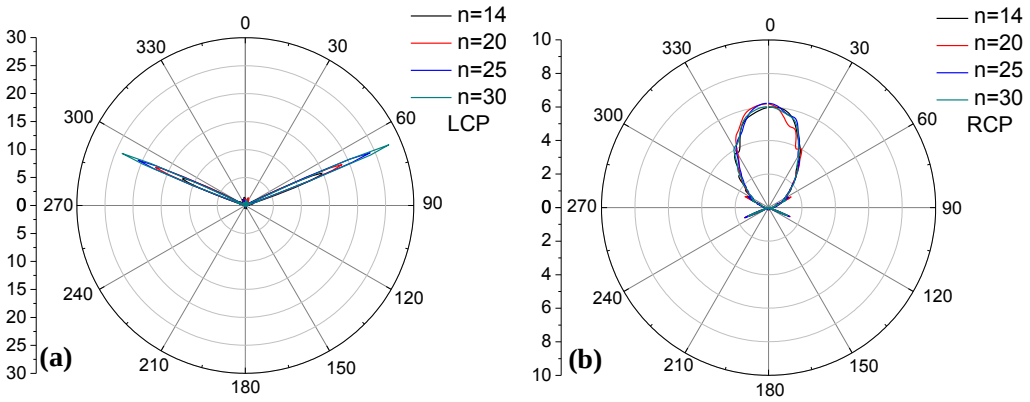

FIG. S7. Simulated far-field radiation patterns (φ = 90°, linear scale) of different *n* for (a) LCP and (b) RCP incident waves at 9 GHz.

III. LEAKAGE CONSTANT α VERSUS FREQUENCY

For LCP incidence case, the leakage constant α versus frequency for the HTW with n =14 and n = 30 (the other geometric parameters of the HTW are: d = 21.6 mm, t = 0.5 mm, s = 4 mm, w = 15 mm, a =19 mm, l = 290 mm corresponding to n =14, and l = 600 mm corresponding to n =30) are calculated, respectively. For the proposed HTW, the expression for the percentage of power radiated is given by $\eta=1-\frac{P(l)}{P(0)}=1-\exp(-2\alpha l)$, where α is leakage constant, P(l) is the power remaining in the leaky mode at z = l and P(0) is the power input at z = 0. With the expression, the calculated leakage constant α versus frequency are shown in Fig. S8.

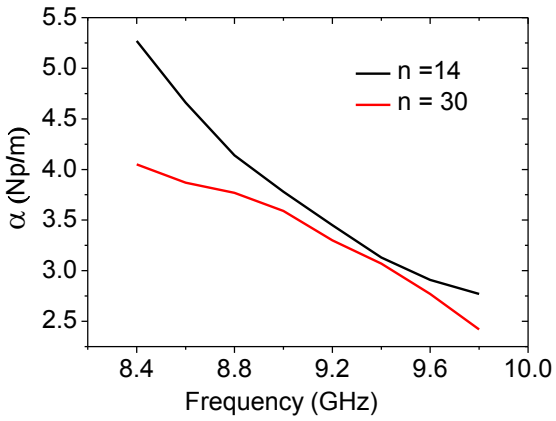

FIG. S8. Leakage constant α versus frequency.

IV. MEASURED REFLECTION SPECTRA

Figure S9 display the measured and simulated reflection spectra of the HTW with n = 14, and n = 30 , respectively. The measured result shows that the reflection is low for both HTW samples, which agrees with the simulations.

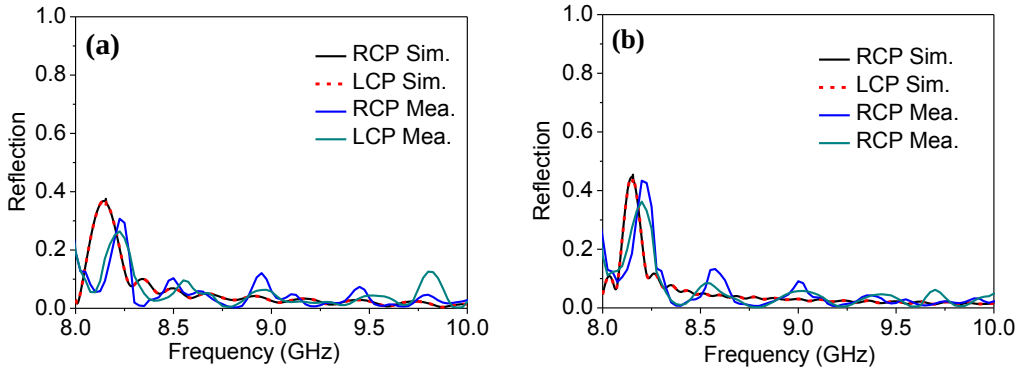

FIG. S9. Reflection spectra for the HTW samples with (a) n =14 and (b) n = 30.